IECON 2024 - 50th Annual Conference of the IEEE Industrial Electronics Society | 978-1-6654-6454-3/24/$31.00 ©2024 IEEE | DOI: 10.1109/IECON55916.2024.10906012

ELECTRICAL & COMPUTER ENGINEERING
UNIVERSITY of WASHINGTON

Alexander V. Mamishev, Ph.D.
Department of Electrical & Computer Engineering
University of Washington, Seattle
215 ECE/CSE Building, Box 352500
Seattle, WA 98195-2500
mamishev@uw.edu
https://www.ece.uw.edu/people/alex-mamishev/
tel 206 221-5729, fax 206 543-3842

19 August 2024

Dear Editor,

Thank you for giving us the opportunity to submit a revised draft of my manuscript titled Miniaturization of High Voltage Power Supply for Portable Electrostatic Filtration to the *Annual Conference of the IEEE Industrial Electronics Society (IECON)*. We appreciate the time and effort that you and the reviewers have dedicated to providing your valuable feedback on my manuscript. We are grateful to the reviewers for their insightful comments on my paper. We have been able to incorporate changes to reflect most of the suggestions provided by the reviewers. We have highlighted the changes within the manuscript. We had to add a page to address all concerns and will pay the extra page charges.

Here is a point-by-point response to the reviewers' comments and concerns.

Comments from Reviewer 1

- **Comment 1:** *[Losses, efficiency, and thermal considerations of the flyback transformer and switching MOSFETs are not analyzed.]*

Response: Thank you for this valuable suggestion. We have added detailed text addressing these considerations in the last two paragraphs of the *Results and Discussion* section.

- **Comment 2:** *[Some discussion on control logic for sequencing, startup, fault protections etc. can be added.]*

Response: Thank you for your feedback. We have incorporated a discussion on control logic for sequencing, startup, and fault protections in the *Conclusions* section.

- **Comment 3:** *[PCB layout and component placement for reducing EMI/noise can be covered, which can be critical for a high frequency design.]*

Response: Thank you for highlighting this aspect. We have addressed the importance of PCB layout and component placement for reducing EMI/noise in the *Conclusions* section.

- **Comment 4:** *[No information is provided on the current driving capability/limits of the flyback stage. This is important for the load characteristics.]*

Response: You have raised an important point. We have added a discussion on the current driving capability and limits of the flyback stage, including its relevance to load characteristics, in the section where operating parameters are explained, particularly in relation to *Figure 8* in the *Results and Discussion* section.

Comments from Reviewer 2

- **Comment 5:** *[Why corona is in the keywords?]*

Response: Thank you for highlighting this point. We included "corona" in the keywords because corona discharge plays a critical role in our study. Specifically, air ionization occurs around the electrodes due to corona discharge, which is a key mechanism in the air-purifying technology utilized by the Mask. Additionally, we have clarified this point in the manuscript just prior to citation 6.

ELECTRICAL & COMPUTER ENGINEERING
UNIVERSITY of WASHINGTON

Alexander V. Mamishev, Ph.D.
Department of Electrical & Computer Engineering
University of Washington, Seattle
215 ECE/CSE Building, Box 352500
Seattle, WA 98195-2500
mamishev@uw.edu
https://www.ece.uw.edu/people/alex-mamishev/
tel 206 221-5729, fax 206 543-3842

19 August 2024

- **Comment 6:** *[Some citations are not in IEEE format e.g. [7,8], [13,16,17].]*

Response: Thank you for bringing this to our attention. We have carefully reviewed and corrected the formatting of the citations to ensure they now adhere to the IEEE style guidelines.

- **Comment 7:** *[End the literature review by describing in short what is going to be discussed in different sections.]*

Response: Thank you for the suggestion. We have now included a brief outline of the subsequent sections at the end of the introduction section to provide a clear overview of the structure of the paper.

- **Comment 8:** *[On every page, images should be either on top or bottom not in between the text. Fig captions are not italicized in IEEE format.]*

Response: Thank you for pointing this out. We have repositioned the images to either the top or bottom of each page, ensuring consistency with IEEE guidelines. Additionally, the figure captions have been unitalicized and corrected to meet the IEEE format requirements.

- **Comment 9:** *[Label the waveforms of the experimental figures in the graph or the caption (Fig. 5).]*

Response: Thank you for your suggestion. The waveforms in *Figure 5* have now been labeled appropriately within the graph and the caption to enhance clarity and meet the required standards.

- **Comment 10:** *[What is the voltage generated at the output of the rectifier that is supplied to the input of the flyback dc-dc converter?]*

Response: Thank you for your question. It appears there may be a misunderstanding. The input to the flyback DC-DC converter is supplied directly by a battery, not by the rectifier. We hope this clarification addresses your concern.

- **Comment 11:** *[The functional block diagram is confusing with the illustration.]*

Response: Thank you for your observation. We agree with your feedback and have revised the functional block diagram using standard electronics symbols instead of blocks to enhance clarity and better align with conventional representation.

- **Comment 12:** *[The switching frequency selected is 20 kHz and the application is mask. The brain will be continuously exposed to EMI and EMC which may be a further challenge for its application. Some comments can be added in this direction.]*

Response: Thank you for raising this important concern. We have addressed this in the second-to-last paragraph of the conclusion, where we discuss the potential impact of EMI and EMC exposure in this application. Relevant references have also been added to support the discussion, including citations from authoritative sources [27, 28].

Citations: https://www.ncbi.nlm.nih.gov/pmc/articles/PMC6513191/ [27]

ELECTRICAL & COMPUTER ENGINEERING
UNIVERSITY of WASHINGTON

Alexander V. Mamishev, Ph.D.
Department of Electrical & Computer Engineering
University of Washington, Seattle
215 ECE/CSE Building, Box 352500
Seattle, WA 98195-2500
mamishev@uw.edu
https://www.ece.uw.edu/people/alex-mamishev/
tel 206 221-5729, fax 206 543-3842

19 August 2024

https://www.who.int/news-room/questions-and-answers/item/radiation-electromagnetic-fields [28]

Additional Clarifications

In addition to the above comments, all spelling and grammatical errors pointed out by the reviewers have been corrected.

We look forward to hearing from you in due time regarding our submission and to responding to any further questions and comments you may have.

Sincerely,

Alexander V. Mamishev, Ph.D.
Professor, Electrical & Computer Engineering
Affiliate Professor, Mechanical Engineering
Director of the Sensors, Energy, and Automation Laboratory
Director of the UW Industrial Assessment Center

Miniaturization of High Voltage Power Supply for Portable Electrostatic Filtration

Jia Hao (Joe) Wang[1], Cynthia Yu[1,3], Cameron Urquhart[2], Zane Hernke[2], Jan Leuca Espelien[4], Christopher Simpson[3], Igor Novosselov[5], Alexander Mamishev[1]

[1]SpectTree, LLC, Seattle, WA, USA / email: joe.w@spectree.com

[2]Department of Electrical and Computer Engineering, University of Washington, Seattle, WA, USA
emails: cynthiia@uw.edu, camurk02@uw.edu, zhernke@uw.edu, mamishev@uw.edu

[3]School of Public Health, University of Washington, Seattle, WA, USA

[4]Dept. of Electrical Engineering, Columbia University, New York, NY, USA / email: jan.l.espelien@gmail.com

[5]Department of Mechanical Engineering, University of Washington Seattle, WA, USA / email: ivn@uw.edu

***Abstract*— Electrostatic Precipitation (ESP) is an effective method of removing particulates from the air. It is currently used in many large-scale industrial applications but sees limited use in smaller-scale cases due to the difficulty of generating high voltage in small packages. Additionally, safety concerns prevent the widespread use of this effective technique. This paper presents the motivation, design, and evaluation of a miniature high-voltage DC (HVDC) power supply for applications in small-scale ESP systems. The power supply's potential for portable ESP application is tested on a personal protective device, the so-called Smart, Individualized, Noncontact, Extended-Wear (SINEW) mask. The results show that the power supply operates with acceptable efficiency and generates high voltages and power necessary to drive ESP setups in practical applications.**

***Index Terms*—Corona, DC-DC power converters, Electrostatic precipitators, high voltage power supplies.**

I. Introduction

Electrostatic precipitators (ESPs) are devices that use an electric field to capture particles from gas streams [1]. They help clean the air and protect people's health by removing air pollutants like dust, smoke, pollen, and volatile organic compounds like bacteria and viruses. Many industrial applications, such as power generation, cement production, metallurgy, and oil refining use ESPs to comply with environmental standards [2]. For instance, ESPs are vital for trapping fine ash particles in coal-fired power plants [3].

ESPs charge suspended particles in the air using corona discharge and collect them through induced Coulombic forces [4]. ESPs typically consist of a 'discharge' electrode and an oppositely charged 'collecting' electrode, separated by a space where air can flow [5]. When a high voltage direct current (HVDC) potential is applied, a strong electric field is produced around the discharge electrode, ionizing the air around it through corona discharge [6]. These ions attach themselves to aerosols and particles suspended in the gas, attracting them to the oppositely charged collecting electrode [3]. The particles then form a solid layer on the collecting electrode, eventually requiring rapping or cleaning the electrode and removing the filtered particles from the ESP [7], [8]. ESPs can operate at efficiencies >99% and effectively collect sub-micrometer particles [9].

The current main limitation of ESPs is their size. As the size of ESPs decreases, numerous new potential applications will become feasible. ESPs have already been developed into portable and miniature versions [10], which are handy for local air purification where large-scale systems are impractical. Furthermore, miniature ESPs are gaining interest in personal air purifiers and other applications, which offer individual-scale solutions for individual exposure to pollutants in localized settings. Some examples of applications of miniaturized ESP technology that are already commercialized are:

- A portable electronic air cleaner called Smog-Hog PCN, by Parker Hannifin Corporation. This device can eliminate particulate matter as it is generated at the source, such as in welding, grinding, or cutting operations. It has a unit-mounted hood that captures the contaminant and conveys it to the precipitator, where it is collected and disposed of [11].

- A portable air purifier, BAPUV350, by Black&Decker [12]. This device uses a four-stage filtration process that includes a pre-filter, an electrostatic precipitator, an ozone filter, and a HEPA-activated carbon combo filter. It can remove up to 99.98% of pollutants, pet dander, gaseous pollutants, dust mites, viruses, bacteria, and pollen as small as 0.30 μm in large rooms up to 46 m^2 [13].

Portable or miniature ESPs have significant advantages over other types of air purifiers, such as HEPA filters or ionizers [14]. They can handle large volumes of gas at high temperatures, have low operating costs, have high collection efficiencies [15], and meet general trends of increasing popularity and usefulness for wearable devices [12].

Financial support for this research effort was provided by JCATI, CoMotion (University of Washington), Washington Research Foundation, and NIOSH Grant 1 R21 OH012599-01.

Other applications that could use ESP technology are solar panel cleaning, indoor filters, and, promisingly, face masks [13], [16], [17]. Given the challenges observed with N-95 masks during the COVID-19 pandemic, there is motivation for developing face mask technology based on ESPs due to their potential advantages in comfort, environmental impact, reusability, and filtration efficiency [18].

This paper discusses specific requirements for ESP applications in personal protective devices in the following sections. Section II outlines the application requirements and the design considerations for a compact high-voltage power supply customized for the SINEW mask. Section III describes the detailed design of the power supply, including its schematics and control circuits. Section IV presents the results of performance testing and discusses the effectiveness of the system. The paper concludes with an evaluation of the overall system's potential and suggestions for future improvements in Section V.

II. Application Requirements

The application discussed in this paper focuses on providing the solution for powering a recently invented personal protective device, the Smart, Individualized, Noncontact, Extended-Wear (SINEW) Mask [19], see Fig. ***1***. The SINEW Mask contains a plasma (as opposed to dielectric barrier discharge) electrostatic precipitator, which relies on a copper wire with a diameter of 1.02 mm as a collection electrode and a copper sheet with sawtooth cutouts at its edges acting as the discharge electrode. The effort described here is the design of a compact DC-DC converter powered by a low-voltage battery that could supply

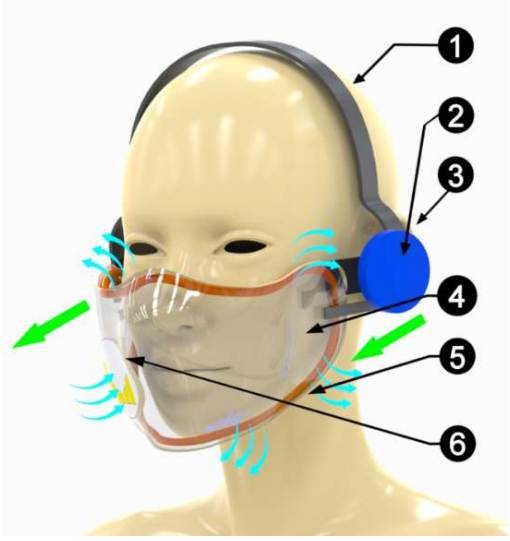

Fig. 1. A 3D model of the SINEW Mask. Particles are removed by an electrostatic filter (5) placed at the perimeter of the mask. The flexible plastic shield surrounding the nose and mouth (4) can be adjusted using the blue mechanical wheel (3). The mask is held on by the head strap (1), which evenly distributes weight and pressure for added comfort. The control unit and battery supply are at the back (2).

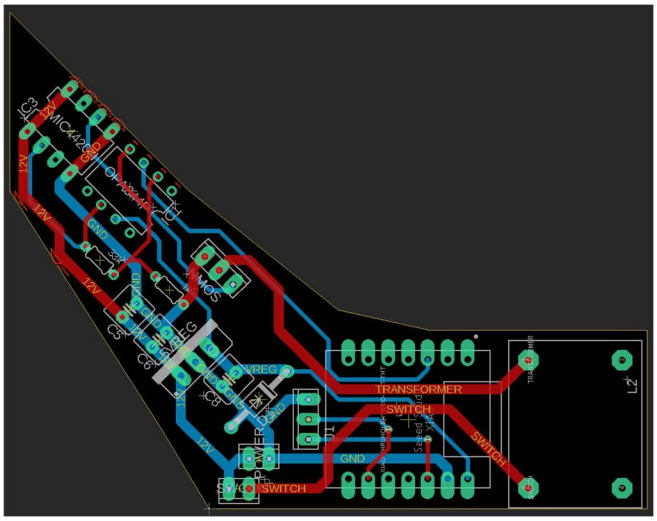

Fig. 2. PCB Layout of the HV power supply has to follow the curved shape of the mask

about 10 kV of negatively biased potential at a peak instantaneous current of roughly 1 mA. Based on this device's power draw requirement, a search for compatible power supplies was conducted to find an affordable, compact, and relatively powerful high-voltage source for the SINEW Mask. The most relevant results are shown in Table 1.

However, none of the dimensions would be ideal for the desired geometry of the mask. The XP-Power series supply is too wide, while the 10A24-N15's requires input voltage is too high to be supplied by most compact Li-Po batteries. In order to accommodate the form factor requirements of the wearable device, a curved-shape circuit board was designed specifically for this application, see Fig. ***4***. Fig. ***3*** shows a photograph of the entire electronics design integrated inside the headband of the face mask. The weight distribution is made to counter the weight of the front plate of the mask that holds the electrodes.

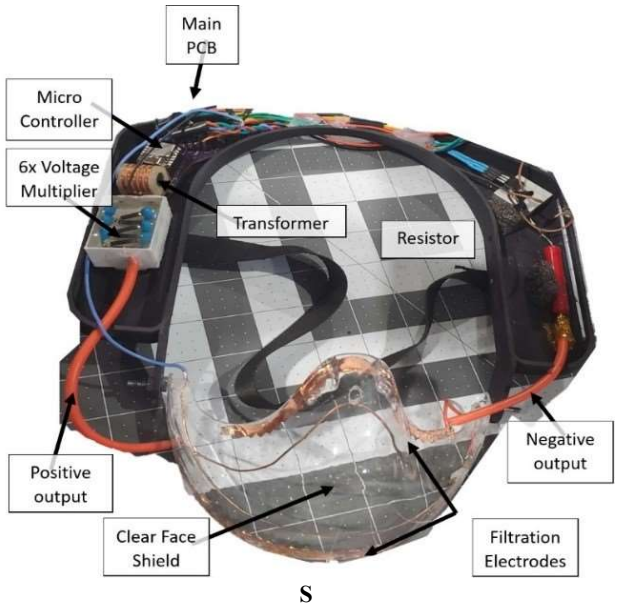

S

Fig. 3. SINEW Mask prototype with electronics' layout and electrodes on the face shield.

III. Power Supply Design

A. Overview of High Voltage DC Supplies

Small HVDC power supplies are generally operated via piezoelectric or flyback mechanisms. Piezoelectric HVDC power supplies have the advantage of not generating significant magnetic fields compared to conventional ferrite core transformers and are also generally lower in profile. However, they are typically more expensive and lower powered than flyback transformers [19].

The design of HVDC converters beyond piezoelectric types is grounded in the principle of creating AC signals, typically stepped up by a transformer and subsequently multiplied. This necessitates the discussion of AC-AC step-up converters. Critical considerations in driving power supplies include voltage levels, power ratings, efficiency, stability, and safety.

The resonant converter is a favored design topology for high-voltage power supplies due to its efficiency and reliability [20], [21]. A commonly known design within this category is the flyback topology, which generates high voltages on the primary side of a transformer with a high turn ratio through inductive kickback. This straightforward switching method has been utilized in various applications, including driving DBD plasmas [22]-[25]. However, hard switching is generally less efficient and generates more noise than soft switching [26].

A limitation of the flyback topology, in addition to the strain on components and reduced efficiency, is the power capacity of the supply itself. All energy released must be stored in the transformer where saturation and heat are serious concerns, especially when attempting to reach maximum power output with minimal space. This issue complicates achieving clean sinusoidal high voltage due to the transformer's low inductance.

During the design process, component size was a primary consideration. It was found that ignition pulse transformers were cost-effective solutions for achieving a high turn ratio, making them well-suited for this application. The chosen transformer is a generic single-pole flyback transformer with a turn ratio 100:1 rated for a 20 kV output. Transformer selection is crucial as its characteristics, combined with the load, determine the optimal operating parameters of the power supply. Using a DE-5000 LCR Meter, the primary resistance, inductance, and capacitance was found to be 130 mΩ, 24.7 µH, and 1022 µF respectively.

Secondary to the transformer, the MOSFETs used for switching are critically important as they manage the bulk of the power passing through the system. One limiting feature of MOSFETs in this application is the device's thermal performance, as in a compact design, there is little space for active cooling or large heat sinks. Therefore, the IRFZ44N MOSFET was chosen for its low $R_{(DS)ON}$ value of 0.028 Ω.

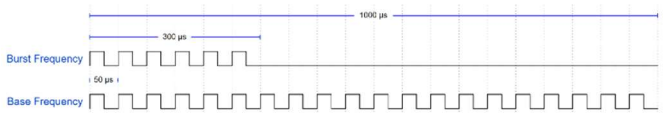

Fig. 5. Theoretical waveform diagram given a base frequency of 20 kHz, duty cycle of 50 %, burst frequency of 1 kHz, and burst ratio of 30 %.

B. Oscillator

In a stable or free-running mode, the LM555 timer can operate as an oscillator and generate a stabilized square waveform of a fixed frequency and duty cycle. However, any variations to frequency or duty cycle require modification of the resistor and capacitor combination, which may be impractical for a final product. Recent microcontrollers like the Seeeduino XIAO have become a cost-effective, high-performance solution for embedded applications while maintaining a compact footprint. It was selected for its compact mass (only 4 g) and dimensions (21 mm by 17.5 mm by 3.5 mm), making it the most suitable microcontroller with the necessary computing frequency to control a fully featured and adjustable control system. Successful microcontroller integration requires analysis of timer counter for control (TCC) applications, software development of frequency and phase correct pulse-width modulation (PWM), and real-time control of frequency, duty cycle, burst frequency, and burst ratio.

C. Control Circuits

Burst frequency modulates a continuous square waveform to allow for intermittent discharge. The typical parameters are the base frequency, duty cycle, burst frequency, and burst ratio. Fig. ***5*** shows a comparison between burst frequency and base frequency given a base frequency of 20 kHz, duty cycle of 50%, burst frequency of 1 kHz, and burst ratio of 30%.

D. Overall Approach and Schematics

The Seeeduino XIAO SAMD21 is an Arduino-compatible development board powered by the SAMD21G18, a 32-bit, 48 MHz microcontroller with an ARM Cortex-M0+ architecture. Multiple pulse-width modulation (PWM) generation methods exist for the SAM D21 chip, but dual-slope PWM was selected to enable frequency and phase-correct PWM. In dual-slope operation, the counter counts from ZERO (BOTTOM) to PER (TOP) and then PER to ZERO. The output compare (OC1x) is set on compare match when up-counting and cleared on compare match when down-counting. During each timer cycle, the counter is incremented until the counter value reaches the

Table 1. *A comparison matrix of commercially available and presented here high voltage power supplies.*

Name	Max Voltage (kV)	Max Current (mA)	Dimensions (mm)	Input DC Voltage (V)
XP Power F-Series DC-HVDC Converter F101R [20]	10	1	71.1 x 43.2 x 21.6	0-15
High Voltage Products 10A24-N15 [e][21]	10	1.5	94.6 x 38.7 x 24.5	24
Micromechatronics 10 kV DC-DC Converter [22]	10	.5	150 x 35 x 20	8-14
SINEW Mask Power Supply	12.1	1	21 x 133 x 20, curved shape	12

TOP value set by the PER register and the count direction changes. This process determines the frequency of the PWM operation, which can be calculated with (1).

$$f_{base} = \frac{48}{2 \times N \times TOP} \quad (1)$$

Other essential variables include N, the clock pre-scaler divider, which divides the CPU clock by 1, 8, 64, 256, or 1024 cycles. With N set to 1, (1) can be simplified and rearranged, as shown in (2).

$$TOP = \frac{48}{2 \times f_{base}} \quad (2)$$

Lastly, the duty cycle of the generated waveform can be adjusted with the CCx register. Given the base frequency and desired duty cycle, this value can be calculated as shown in (3).

$$CCx = \frac{48 \times D}{2 \times f_{base}} \quad (3)$$

Within the dual-slope operation of the SAMD21, the DUAL_SLOPE_BOTTOM configuration is selected to generate an interrupt each time the counter reaches the ZERO (BOTTOM) value. T_{burst}, the period of the desired burst frequency is used to pause the execution of the interrupt service routine (ISR) continuously, as shown in (4).

$$T_{burst} = \frac{1}{f_{burst}} \quad (4)$$

BR, the desired burst ratio, T_{base}, the period of the base frequency, and T_{burst}, the period of the burst frequency, are compared to determine the required number of pulses for the burst waveform, as shown in (5).

$$n_{pulses} = \frac{T_{burst} \times BR}{T_{base}} \quad (5)$$

Inside the ISR, a counter increments up to n_{pulses} as calculated in (5). Once the counter reaches n_{pulses}, the ISR execution is paused for the duration of T_{burst}. During testing, four 10 $k\Omega$ potentiometers, the frequency and duty cycle of the base frequency waveform, as well as the burst frequency and burst ratio of the burst frequency waveform, can be adjusted from 0 kHz to 50 kHz, 0% to 100%, 0 kHz to 10 kHz, and 0% to 100%, respectively. PA10 or digital pin 2 of the Seeeduino XIAO contains the PWM output, see top waveform of Fig. ***6***.

The rectification and multiplication of the HV AC power to HVDC was accomplished using a custom 6-stage Cockcroft Walton voltage multiplier, potted in an enclosure designed to fit the SINEW mask. The block diagram of the high-voltage power supply (HVPS) is displayed in Fig. *7*. Since miniaturization is the design's primary concern, supplying the multiplier with high-frequency high voltage AC was the flyback geometry previously mentioned. The final design is placed on a curved PC board, measuring 21 mm in width by 133 mm in length and weighing 65 g. The schematic is shown in Fig. ***8***. Additionally, it was decided that the unit would be powered by a 3-cell 11.1V LiPo battery, which was found to be a good fit for the mask team's desired layout. A 500 MΩ discharge resistor is placed between the ground and the high-voltage electrode to discharge the capacitive voltage multiplier when the device is turned off.

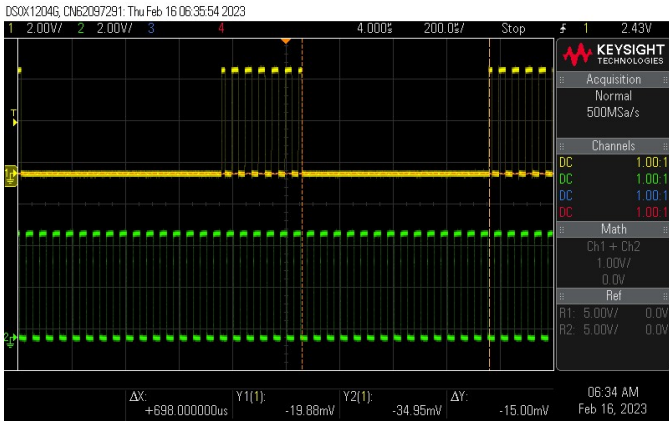

Fig. 6. Green PWM waveform (top) displays a base frequency. Yellow waveform displays (bottom) burst waveform of the base frequency. The duty ratio changes based on minor geometry variations and environmental conditions.

IV. Basic Performance

As shown in Fig. ***3***, a face shield with flat sawtooth-shaped copper electrodes situated along its entire perimeter completes this version of the face mask prototype. The electrodes are affixed with a uniform 14 mm gap, with consistent spacing across the entirety of the face shield. In this paper, the remaining discussion is focused on the performance of the power supply, and the experimental results with the face mask, such as the filtering efficiency, will be reported in later publications.

The variables of interest include the base frequency applied to the transformer, the frequency's duty cycle, and the voltage multiplier's strength. Following a series of tests, a 6x voltage multiplier was optimal, striking a balance between achieving sufficiently high voltage levels and minimizing voltage losses.

The voltage waveforms at different power supply stages were measured with an oscilloscope to establish the base frequency and duty cycle parameters. We employed an AC high-voltage probe across various duty cycles and a broad spectrum of frequencies. A range from 15 kHz to 40 kHz at a 25% duty cycle

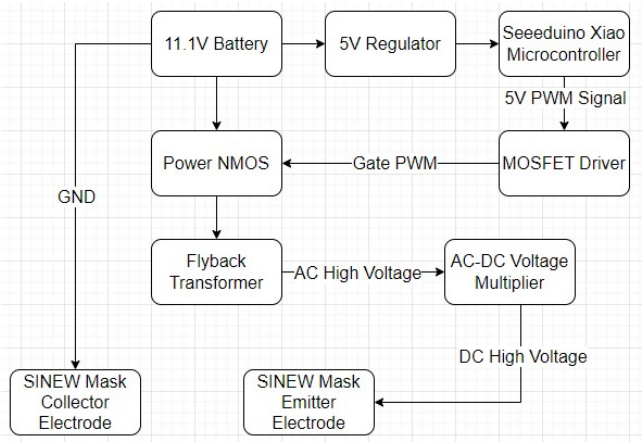

Fig. 7. Simple HV flyback power supply functional diagram.

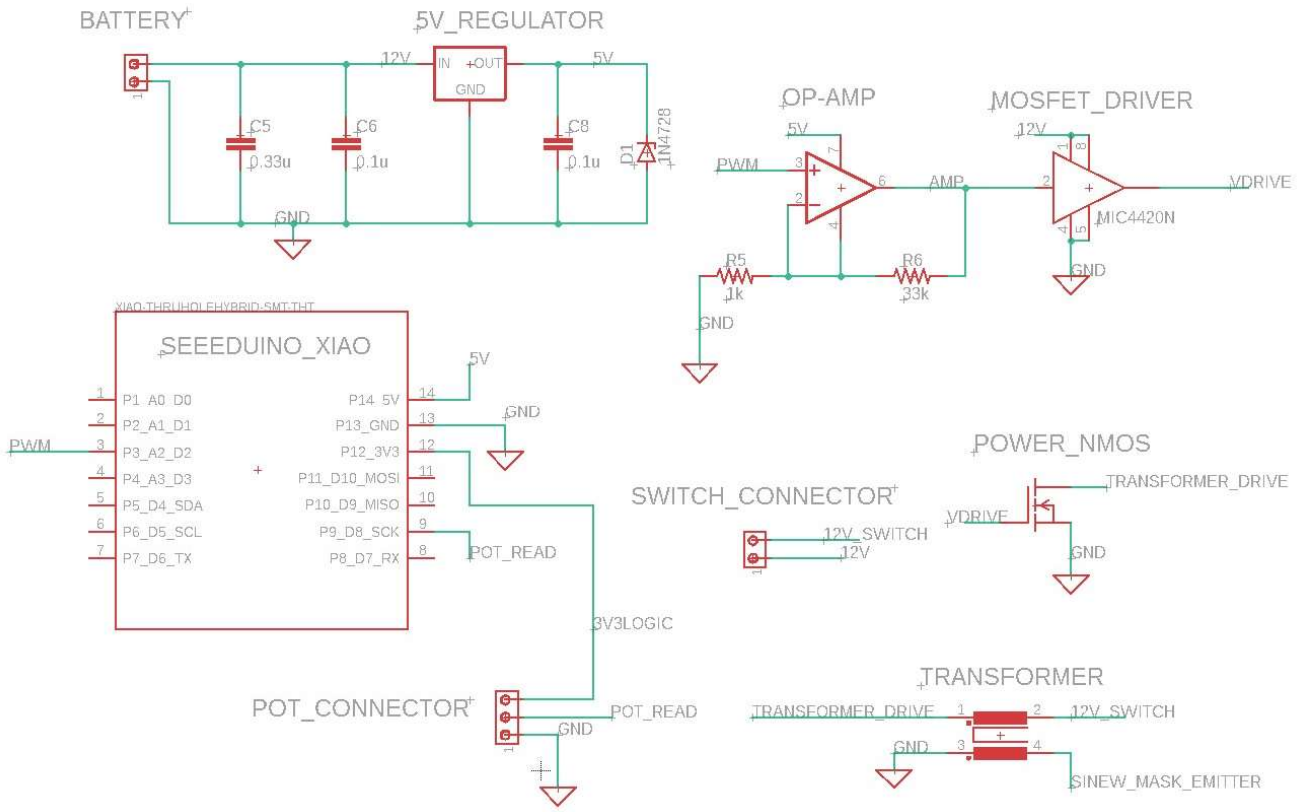

Fig. 8. Schematic of the SINEW Mask high voltage power supply.

was selected, where the burst frequency can be tuned during use by an external potentiometer dial. Through adjusting the base frequency, the flyback voltage was altered, thus allowing for live control of the HVDC output. With these parameters, the power supply was limited to -7.7 kV to -12.1 kV based on potentiometer control to avoid arcing between mask electrodes. It was decided that the low-frequency burst function was to be kept in the final mask to decrease power draw, allowing the oscillator and transformer to operate at more optimal pulses to generate high voltage and then shut off to allow the mask to discharge, generating a negative DC-biased sawtooth waveform. This base duty cycle and frequency were also adjusted based on experimental trial and error but remain wholly adjustable through software.

Fig. 9. Waveforms of flyback transformer voltage output. The yellow line represents the high-voltage AC waveform at the transformer. The red line shows the current output with 1 V = 1 A. The blue line shows the PWM signal that drives the power MOSFET.

V. Results & Discussion

The power supply designed met the requirements of the application. While it can charge the ESP and filter particles effectively, power consumption and electrical characteristics are important for future design considerations and understanding its long-term operational capability.

Operating at 12 V, measurement of the battery drain during active use using a digital ammeter shows power consumption of 2.1 W. With the 22.2 Wh battery used, an expected use time per charge of 10.6 hours is expected. Based on Ohms Law, 0.2 W of the power is lost to the 500MΩ discharge resistor, assuming a 10 kV potential, and the rest of the power consumption is assumed to be due to thermal losses and corona discharge, the ratio of which has yet to be explored. Fig. ***9*** shows the correlation between the PWM signal and the current output. While inconsequential for the eventual voltage output shown in **Error! Reference source not found.**, because the operation is essential DC, the important feature of this design is the ease of adjusting the base DC voltage level dynamically in complex portable and wearable applications. Unlike industrial filters that do not have to adjust to changes in external geometry, this

Fig. 10. Waveforms of SINEW Mask emitter electrodes. The red line shows the current output with 1 V = 1 A. The blue line (top) shows the PWM signal that drives the power MOSFET.

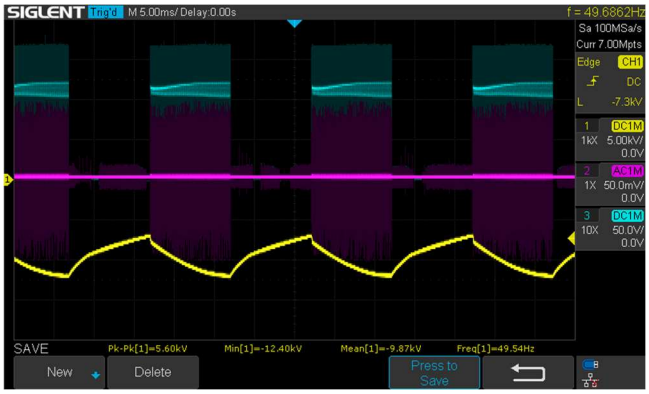

Fig. 11. Waveforms of SINEW Mask emitter electrodes. Showing pulsed operation of PWM and its effects on electrode DC output. The red line shows the current output with 1 V = 1 A. The blue line (top) depicts the PWM signal that drives the power MOSFET.

application presents the challenge of external objects in the vicinity of the electrodes.

Fig. ***11*** shows the measurement of voltage indicated by the yellow line in 500V/div scaling. As measured using an RF-compensated Rogowski coil, the purple line indicates the current, where 1 A is equivalent to 1 V measured by the oscilloscope. During operation, the ESP electrodes were measured by a Tektronix P6015A RF compensated High Voltage probe read by a GW Instek GDS-1052-U Digital Storage oscilloscope. The measurements show a voltage potential of 9 kV to 16.3 kV DC at a 25% duty cycle.

At these operating parameters, the mask can drive the capacitive and resistive load of the half-wave series multiplier. This load consists of a 100pF load of the capacitors in the multiplier, and the rectifying diodes within. At this load, the flyback stage generates a 2.6 kV peak-to-peak voltage of a roughly sawtooth nature, with a charging current of roughly 40 mA. Outside of this specific load case and application, the flyback stage's output characteristics have not been thoroughly explored due to time limitations, and the scope of this paper for driving the low capacitance voltage multipliers.

The thermal performance of the device is essential as it is to be placed close to persons and is mounted within a nylon enclosure, which is sensitive to heat. General observation of the device found that heat generation was not a significant issue at such a low power level. Extensive calculations of efficiency were not considered necessary for application at this stage, but they would provide insight for future work. A rough conductance loss calculation and switching loss calculation will be done to gain a rough understanding of device efficiencies, however.

The calculated average current draw while the device is on is calculated to be 0.18 A, based on a 12 V source and the 2.1 W measured power draw. However, because of an overall duty cycle of roughly 12.5%, formed by a roughly 50% burst duty cycle, and the 25% base duty cycle – the actual average current during switching is 1.4 A, as all significant current draw occurs during the 12.5% of cycle. With the total series resistance of the MOSFET and transformer primary being roughly 0.16 Ω, conductance losses are calculated to be 0.31 W during positive duty cycles and an average of 0.039 W when the supply is on.

Rough switching losses can be approximated by the product of switching charge and switching frequency, although this does omit the power loss at the gate-drive mechanism. Using a figure of 67 nC of the max gate charge according to the IRFZ44's datasheet, and a switching frequency of 15 kHz , or 30 kHz at a 50% burst duty cycle, average switching current is 1 mA, resulting in a switching loss of roughly 12 mW. Due to this system's low frequency operation, it is consistent that most significant losses are from conduction.

VI. Conclusions

The miniature DC high-voltage power supply designed for small-scale ESP systems, particularly the SINEW mask, has demonstrated promising results. Despite the challenges of generating high voltage in small packages, the power supply successfully met the requirements set by the team, providing upwards of 10 kV of negatively biased potential at a current of roughly 1 mA.

Utilizing a compact flyback topology, the power supply achieved acceptable efficiency and generated the necessary voltages and power to drive ESP, even on non-optimized geometries. Subsequent publications will discuss the SINEW mask's experimental results that show its filtration efficiency above 90% for specific particle sizes. Additionally, electrical measurements indicated a power consumption of 2.1 W during active use, with an expected use time of 10.6 h per charge, making it suitable for portable applications.

The design, however, has much space for improvement. Startup behavior is crude – relying on to separate switches to power up the device and then connect the NMOS to the transformer. This feature is designed to allow for safe diagnosis and a method to bypass microcontroller startup faults. This method is, however, susceptible to user error in the case the power switch is left on and does not offer shorting or other fault protections, which are important considerations for future work.

EMI considerations are a concern when power electronics and RF signals are concerned. However, rough testing using a TinySA Ultra Spectrum Analyzer has shown little to no discernable change in the MF through UHF bandwidths when the supply is turned on, and testing of the device alongside devices using Wi-Fi and Bluetooth has not incurred any complications. The EMI also does not significantly affect the performance of the board, with no shielding of the transformer or the PCB being required for its stable operation. Despite these encouraging factors, proper EMI characterization, testing, and certification done to industry standard will need to be conducted prior to use outside of a research setting.

EMI and EMC are also a matter of concern to some regarding their biological impact – particularly their effect on the human brain. While there are many studies on the effect of RF-EMF on the brain, from thermal effects, blood-brain-barrier albumin leaks, cancer risk, and more, the results are generally agreed to be inconclusive [27], which is also reflected in EMF health recommendations through official bodies such as the WHO [28]. Therefore, while the power supply's EMF cannot be discounted in regards to its potential health effects on a user, it also does not pose a special risk outside of that tolerated via exposure to other commonplace sources of EMF regarding brain stimulation. Note that the high electric field only exists in the region directly in the vicinity of the high voltage electrodes.

Overall, developing and evaluating this miniature power supply represents a significant advancement in making ESP technology practical for smaller-scale applications. With further optimization and refinement, portable ESP systems like the SINEW mask could offer practical solutions for personal air purification and other localized pollutant removal.

VII. Acknowledgements

Special thanks to Edward Martija for developing the experimental setup for the SINEW mask and ensuring precise particle containment and measurement accuracy.

We would also like to thank Electroimpact, specifically David Zieve, as well as Greg Gaub (Greg's Super Duper THREE DEEE Printing Services) for their assistance with printing our 3D frame designs.

Thanks to Felix Tse, Haoran Lu, Harry Ge, Karlen Aleksanyan, Qifeng Yang, William Hong, and Wei-Chieh Sun for their help in experimental efforts and making editorial contributions to the text for this manuscript.

References

[1] A. Mizuno, "Electrostatic precipitation," *IEEE Transactions on dielectrics and electrical insulation,* vol. 7, no. 5, pp. 615-624, 2000.

[2] W. Zhou, R. Jiang, Y. Sun, B. Chen, and B. Liu, "Study on multi-physical field characteristics of electrostatic precipitator with different collecting electrodes," *Powder technology,* vol. 381, pp. 412-420, 2021.

[3] T.-Y. Wen, H.-C. Wang, I. Krichtafovitch, and A. V. Mamishev, "Novel electrodes of an electrostatic precipitator for air filtration," *Journal of Electrostatics,* vol. 73, pp. 117-124, 2015.

[4] R. S. Vaddi, Y. Guan, A. Mamishev, and I. Novosselov, "Analytical model for electrohydrodynamic thrust," *Proceedings of the Royal Society A,* vol. 476, no. 2241, p. 20200220, 2020.

[5] J. Mo, E. Tian, and J. Pan, "New electrostatic precipitator with dielectric coatings to efficiently and safely remove sub-micro particles in the building environment," *Sustainable Cities and Society,* vol. 55, p. 102063, 2020.

[6] H. Lee *et al.*, "Development of electrostatic-precipitator-type air conditioner for reduction of fine particulate matter in subway," *IEEE Transactions on Industry Applications,* vol. 58, no. 3, pp. 3992-3998, 2022.

[7] T. Banthoengjai, T. Wiangtong, N. Pattanadech, and P. Pannil, "Effect of Rapping Frequency and Intensity in Electrostatic Precipitator Efficiency," in *2023 9th International Conference on Engineering, Applied Sciences, and Technology (ICEAST)*, 2023: IEEE, pp. 136-139.

[8] E. Jaroudi, I. Stretenovic, G. Evans, and H. Tran, "Factors affecting particulate removal efficiency of kraft recovery boiler electrostatic precipitators: a technical review," 2018.

[9] C. Ghazaly, M. Guillemot, B. Castel, E. Langlois, M. Etienne, and M. Hebrant, "Real-Time Optical Ozone Sensor for Occupational Exposure Assessment," in *2019 20th International Conference on Solid-State Sensors, Actuators and Microsystems & Eurosensors XXXIII (TRANSDUCERS & EUROSENSORS XXXIII)*, 23-27 June 2019 2019, pp. 1403-1406, doi: 10.1109/TRANSDUCERS.2019.8808516.

[10] A. Miller, G. Frey, G. King, and C. Sunderman, "A handheld electrostatic precipitator for sampling airborne particles and nanoparticles," *Aerosol Science and Technology,* vol. 44, no. 6, pp. 417-427, 2010.

[11] P. H. Corporation, "Smog-Hog® Portable Electrostatic Precipitator Owner's Manual," *Parker*.

[12] X. Cheng and M. Mamishev, "Characterization of a Wearable LiDAR Sensor for Social Distancing," in *2022 IEEE IAS Global Conference on Emerging Technologies (GlobConET)*, 2022: IEEE, pp. 115-120.

[13] Black+Decker, "14 in. Electrostatic Precipitator Air Purifier," *BLACK+DECKER*.

[14] J.-H. Sung, M. Kim, Y.-J. Kim, B. Han, K.-J. Hong, and H.-J. Kim, "Ultrafine particle cleaning performance of an ion spray electrostatic air cleaner emitting zero ozone with diffusion charging by carbon fiber," *Building and Environment,* vol. 166, p. 106422, 2019.

[15] S. Gao and B. Xie, "The guarantee strategy for reliable operation of the precipitation with mobile electrode electrostatic technology," in *Modern Econ Manage Forum*, 2020, vol. 1, no. 1.

[16] M. G. Hudedmani, G. Joshi, R. Umayal, and A. Revankar, "A comparative study of dust cleaning methods for the solar PV panels," *Advanced Journal of Graduate Research,* vol. 1, no. 1, pp. 24-29, 2017.

[17] R. K. Redmann *et al.*, "A miniaturized electrostatic precipitator respirator effectively removes ambient SARS-CoV-2 bioaerosols," *Viruses,* vol. 14, no. 4, p. 765, 2022.

[18] J. M. Segovia, C.-H. Huang, M. Mamishev, N. Yuan, J. He, and I. Novosselov, "Performance of textile mask materials in varied humidity: Filtration efficiency, breathability, and quality factor," *Applied Sciences,* vol. 12, no. 18, p. 9360, 2022.

[19] S. Bushwick, "Better Face masks are possible: Here are some winning designs," ed. Scientific American: Scientific American, 2022.

[20] X. P. Power, "XP Power F Series DC-HVDC Converter," in *COMPACT, I/O PROPORTIONAL HIGH VOLTAGE POWER SUPPLIES 10W, F SERIES*.

[21] H. V. Products, "A series - HVP: High voltage products gmbh," *HVP High Voltage Products*.

[22] I. Micromechatronics, "High Voltage Piezoelectric DC-DC converters," *Micromechatronics, Inc*.

IECON 2024 - 50th Annual Conference of the IEEE Industrial Electronics Society | 978-1-6654-6454-3/24/$31.00 ©2024 IEEE | DOI: 10.1109/IECON55916.2024.10905189

IECON 2024- 50th Annual Conference of the IEEE Industrial Electronics Society

Proceedings

Sheraton Grand Chicago Riverwalk

Chicago, Illinois, USA
3 - 6 November 2024

Sponsored by

IEEE Industrial Electronics Society (IES)

IEEE Catalog Number: CFP24IEC-ART
ISBN: 978-1-6654-6454-3